

Enhanced two-photon emission from a dressed biexciton

Carlos Sánchez Muñoz,¹ Fabrice P. Laussy,^{1,2} Carlos Tejedor,¹ and Elena del Valle¹

¹*Departamento de Física Teórica de la Materia Condensada and Condensed Matter Physics Center (IFIMAC),
Universidad Autónoma de Madrid, 28049, Spain.*

²*Russian Quantum Center, Novaya 100, 143025 Skolkovo, Moscow Region, Russia*

(Dated: November 17, 2021)

Radiative two-photon cascades from biexcitons in semiconductor quantum dots under resonant two-photon excitation are promising candidates for the generation of photon pairs. In this work, we propose a scheme to obtain two-photon emission that allows to operate under very intense driving fields. This approach relies on the Purcell enhancement of two-photon virtual transitions between states of the biexciton dressed by the laser. The richness provided by the biexcitonic level structure allows to reach a variety of regimes, from antibunched and bunched photon pairs with polarization orthogonal to the driving field, to polarization entangled two-photon emission. This evidences that the general paradigm of two-photon emission from a ladder of dressed states can find interesting, particular implementations in a variety of systems.

PACS numbers: 42.50.Pq, 03.67.Bg, 78.67.Hc, 42.50.Dv

INTRODUCTION

The generation of non-classical states of light is a major goal in the implementation of photonic quantum technologies [1, 2]. A case of particular interest is the generation of photon pairs, since they present a wide range of applications in quantum information and quantum communications [3]. Photon pairs are an important resource to generate heralded single photons [4] and are also used as a key element for quantum key distribution [5, 6], quantum teleportation [7, 8] or to implement entanglement swapping and quantum repeaters [9–11]. Numerous other examples, like quantum lithography [12], the absorption rate increase from organic molecules in two-photon microscopy [13, 14], quantum walks of correlated photons [15] or the quantum computation of molecular properties [16], illustrate the rich variety of applications that these non-classical states of light can find.

Despite having such an impressive number of applications, the number of ways in which these states can be generated is limited: most sources of photon pairs employed to date are based on parametric down-conversion [3, 7, 16–18]. This mechanism can be implemented in several platforms, and thankfully for prospective technologies, semiconductors are demonstrating excellent performances [19–21]. These sources suffer however from the major drawback that the number of photon pairs generated in each process shows Poissonian statistics, with a non-zero probability of having zero or more than one pair [22]. Promising candidates to overcome this difficulty are quantum emitters that naturally emit entangled photon pairs in a radiative cascade [23]. In the semiconductor case, the biexciton $|B\rangle$ in a quantum dot offers such an implementation, and emission of entangled photon pairs from the biexcitonic cascade has been demonstrated in recent years [24–28]. As an alternative to off-resonant excitation, it is possible to initialize

the biexcitonic state by coherent two-photon excitation (TPE) [28–32], which increases the coherence and indistinguishability of the emitted photons as compared to non-resonant pumping. The generation efficiency and the indistinguishability of the photons can also be improved by bringing a cavity in resonance with the biexcitonic transition [27] to enhance the emission thanks to the Purcell effect [33]. A particularly interesting possibility is to place the cavity in resonance with half the energy of the biexciton to enhance the rate of spontaneous two-photon emission, such that two photons are emitted simultaneously into the cavity mode [34–36]. The joint implementation of coherent excitation and Purcell enhancement via cavity modes has already been discussed in the literature and shown to be promising [28, 35].

Under coherent excitation, the intensity of the pumping sets a limit to the repetition rate of two-photon generation, since strong driving fields dress the excitons and spoil the biexcitonic structure [37, 38]. On the other hand, a recent proposal [39] took advantage of such a dressing and demonstrated that a continuous source of N -photon states—with photon pairs as the simplest realization—can be achieved in precisely this regime of strong admixing of the exciting laser with the emitter. This relies on a family of virtual two-photon transitions, so-called *leapfrog* processes [40], in the strong driving of resonance fluorescence. Since virtual two-photon states are emitted away from the fluorescence peaks, they have a very small probability to occur on their own. These elusive photons are however precious [41] since they feature giant quantum correlations and violate classical inequalities [42]. Despite their scarcity, their existence has recently been demonstrated experimentally by measurements of frequency-resolved photon correlations [43]. It is therefore timely to capitalize on these photons to devise bright, continuous sources of photon pairs by harvesting them with a cavity mode, with a Purcell-effect

applied similarly to previous enhancements of quantum correlations [44, 45] from real photons emitted at the sidebands [46–48].

In this work, we bring together the three main ideas exposed above: i) TPE from the biexciton, ii) cavity Purcell-enhancement of virtual processes and iii) multi-photon emission from a dressed system. This realizes a versatile two-photon source operating in the continuous regime with a high repetition rate. In comparison with the case of a single dressed two-level system, the biexciton introduces an extra degree of freedom, the polarization, that provides a richer set of physical regimes. In particular, we demonstrate the emission of degenerate photon pairs with polarization orthogonal to the laser—therefore suppressing the laser background and undesired excitation of the cavity—and different two-photon counting statistics, as well as emission of polarization-entangled photons. All these different regimes can be accessed optically with the same sample just by changing the intensity and polarization of the excitation. This unprecedented versatility will push forward the generation and use of photon pairs in the laboratory. Even more importantly, it evidences that the fundamental concepts are susceptible to be applied in different platforms, such as superconducting circuits [49], and that new regimes of non-classical light emission are within reach with variations of the design.

Our analysis starts with a general introduction of the model and follows with a detailed description of the features of the dressed biexciton alone, to finally move to the complete picture with the inclusion of a cavity that probes and enhances the single and two-photon transitions present in the dressed system.

MODEL AND DRESSED STATE PICTURE

The system under consideration is a semiconductor quantum dot with a biexcitonic structure, as depicted in Fig. 1(a). The Hamiltonian of this system is given by:

$$H_X = \omega_X(\sigma_\uparrow^\dagger\sigma_\uparrow + \sigma_\downarrow^\dagger\sigma_\downarrow) - \chi(\sigma_\uparrow^\dagger\sigma_\uparrow\sigma_\downarrow^\dagger\sigma_\downarrow), \quad (1)$$

where $\{\sigma_\uparrow, \sigma_\downarrow\}$ are the annihilation operators of the excitons with spin $\{\uparrow, \downarrow\}$, ω_X is the excitonic energy (we consider degenerate excitons) and χ is the biexcitonic binding energy. The biexciton frequency is, therefore, $\omega_B = 2\omega_X - \chi$. To separate the four-level system into two different polarization cascades we change to the linear polarization basis:

$$|H\rangle = \frac{1}{\sqrt{2}}(|\uparrow\rangle + |\downarrow\rangle), \quad |V\rangle = \frac{1}{\sqrt{2}}(|\uparrow\rangle - |\downarrow\rangle) \quad (2)$$

with the annihilation operators

$$\sigma_H = \frac{1}{\sqrt{2}}(\sigma_\uparrow + \sigma_\downarrow), \quad \sigma_V = \frac{1}{\sqrt{2}}(\sigma_\uparrow - \sigma_\downarrow). \quad (3)$$

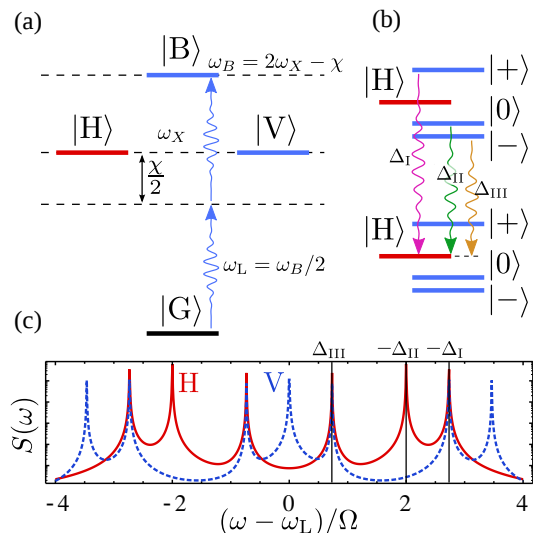


FIG. 1: (Color online) (a) Biexcitonic level system in the linear polarization basis (Horizontal-Vertical states). The two-photon laser excitation is represented with two curly blue arrows, at half the biexciton energy $\omega_L = \omega_X - \chi/2$. (b) Dressed state picture at strong laser pumping, where the vertical polarization states (blue) transform into the new states $|\pm\rangle, |0\rangle$. The three possible horizontally polarised transitions from these states to the $|H\rangle$, appear with curly arrows. (c) Spectrum of emission in the two polarizations, horizontal (solid red) and vertical (dashed blue), and the three horizontally polarised transitions marked with vertical lines. Parameters: $\Omega = 5 \times 10^2\gamma$, $\chi = 2 \times 10^3\gamma$ and $g = 0$.

These operators describe transitions from the biexciton to an excitonic state or from an exciton to the ground state by emission of photons with the corresponding horizontal or vertical polarization (red and blue colors in Fig. 1). We will neglect the small fine structure splitting in frequency that is usually found between the two different excitonic states, since it has no impact in our scheme and only complicates the algebra. It can be trivially added if needed.

We implement a continuous resonant excitation of this level structure that affects only one of the polarizations (chosen to be the vertical one without loss of generalization). This is accounted for by a coherent driving term in the Hamiltonian:

$$H_\Omega = \Omega(\sigma_V^\dagger e^{-i\omega_L t} + \sigma_V e^{i\omega_L t}) \quad (4)$$

where Ω represents the intensity of the exciting laser. In order to drive the biexciton state directly, the laser frequency is set at the two-photon resonance, $\omega_L = \omega_B/2$. This results in a two-photon excitation (TPE) to the biexciton level [28–32]. On the other hand, we gather and enhance the emission in the perpendicular polarization (horizontal) through the coupling to a cavity mode with the same linear polarization. This way, we completely separate in polarization the excitation and emis-

sion channels and do not need to worry about the elastically scattered light from the laser. The coupling to the cavity mode is given by the Hamiltonian term:

$$H_C = \omega_C a^\dagger a + g(a^\dagger \sigma_H + a \sigma_H^\dagger) \quad (5)$$

We write the total Hamiltonian in the rotating frame of the exciting laser:

$$H = H_0 + H_\Omega + H_C = \Delta_X(\sigma_H^\dagger \sigma_H + \sigma_V^\dagger \sigma_V) - \chi \sigma_H^\dagger \sigma_H \sigma_V^\dagger \sigma_V + \Omega(\sigma_V^\dagger + \sigma_V) + \Delta_C a^\dagger a + g(a^\dagger \sigma_H + a \sigma_H^\dagger) \quad (6)$$

where $\Delta_X = \omega_X - \omega_L$ and $\Delta_C = \omega_C - \omega_L$. The dynamics of the whole system is described by a density matrix which follows the master equation:

$$\dot{\rho} = -i[H, \rho] + \frac{\kappa}{2} \mathcal{L}_a \rho + \frac{\gamma}{2} \sum_{X=H,V} [\mathcal{L}_{|X\rangle\langle B|} + \mathcal{L}_{|G\rangle\langle X|}] \rho \quad (7)$$

where we use the definition of the Lindblad term:

$$\mathcal{L}_O \rho = 2O\rho O^\dagger - O^\dagger O \rho - \rho O^\dagger O, \quad (8)$$

and the excitonic and cavity lifetimes are given by γ and κ respectively. We study the steady state of the system defined by $\dot{\rho} = 0$.

Under TPE ($\Delta_X = \chi/2$), the energy of the photons from the laser matches half the biexciton energy, c.f. Fig. 1(a). To understand the spectral features of the system before coupling it to the cavity ($g = 0$), we derive a dressed state picture for the biexciton [37]. The starting point is the set of bare states with n excitations, $\{|G\rangle|n\rangle, |V\rangle|n-1\rangle, |H\rangle|n-1\rangle, |B\rangle|n-2\rangle\}$, where $|n\rangle$ describes the state of the driving field with n photons. Since the laser is polarized in the vertical direction, the state $|H\rangle$ is not dressed by it, while the rest of the excitonic states are. The new eigenstates are obtained by diagonalising the coupling Hamiltonian H_Ω (in the rotating frame of the laser) in the reduced basis $\{|G\rangle|n\rangle, |V\rangle|n-1\rangle, |B\rangle|n-2\rangle\}$, that is, the matrix:

$$H_{\text{TPE}} = \begin{pmatrix} 0 & \Omega & 0 \\ \Omega & \chi/2 & \Omega \\ 0 & \Omega & 0 \end{pmatrix}. \quad (9)$$

We do not include dissipation in this procedure since we consider it small as compared to Ω . This gives rise to the three new eigenvectors $\{|+\rangle, |0\rangle, |-\rangle\}$ in each rung with the corresponding eigenenergies:

$$\Delta_+ = \frac{1}{4} \left(\sqrt{\chi^2 + 32\Omega^2} + \chi \right), \quad (10a)$$

$$\Delta_0 = 0, \quad (10b)$$

$$\Delta_- = -\frac{1}{4} \left(\sqrt{\chi^2 + 32\Omega^2} - \chi \right), \quad (10c)$$

where the eigenvectors, dropping the photonic component from the notation, are given by $|+\rangle \propto |G\rangle + \Delta_+/\Omega|V\rangle + |B\rangle$, $|0\rangle = (|B\rangle - |V\rangle)/\sqrt{2}$ and $|-\rangle \propto |G\rangle + \Delta_-/\Omega|V\rangle + |B\rangle$. Figure 1(b) depicts two successive rungs of excitation, including the state $|H\rangle$ which, as we said, remains bare.

SINGLE PHOTON TRANSITION AND SPECTRUM

The spectrum of emission of the system in each polarization in the steady state, $S_X(\omega)$, with $X=H, V$, is defined as $S_X(\omega) = \Re \int_0^\infty \langle \sigma_X^\dagger(0) \sigma_X(\tau) \rangle e^{i\omega\tau} d\tau$. Both polarizations are plotted in Fig. 1(c) for comparison. The number of peaks appearing and their positions can be explained in each polarization X by the allowed single photon transitions under the operator σ_X . In the case of H polarization, only transitions between $|H\rangle$ and the dressed states $i = +, 0, -$ are allowed: $|\langle H|\sigma_H|i\rangle|^2 \neq 0$ or $|\langle i|\sigma_H|H\rangle|^2 \neq 0$. The transition $|H\rangle \rightarrow |H\rangle$ or between dressed states $|i\rangle \rightarrow |j\rangle$ are forbidden in H polarization, since $\langle H|\sigma_H|H\rangle = 0$ and $\langle i|\sigma_H|j\rangle = 0$ for all $i, j = +, 0, -$. The three possible transitions that can take place from the dressed states to $|H\rangle$, occur respectively at the following detunings from the laser (see Fig. 1(b)):

$$|+\rangle \rightarrow |H\rangle : \Delta_{\text{I}} = \frac{1}{4} \left(\sqrt{\chi^2 + 32\Omega^2} - \chi \right), \quad (11a)$$

$$|0\rangle \rightarrow |H\rangle : \Delta_{\text{II}} = -\chi/2, \quad (11b)$$

$$|-\rangle \rightarrow |H\rangle : \Delta_{\text{III}} = -\frac{1}{4} \left(\sqrt{\chi^2 + 32\Omega^2} + \chi \right). \quad (11c)$$

The other three possible H -polarised transitions take place from $|H\rangle$ to the dressed states, at opposite detunings $-\Delta_{\text{I}}$, $-\Delta_{\text{II}}$ and $-\Delta_{\text{III}}$. Remarkably, $S_H(\omega)$ does not present any resonance at the laser energy.

On the other hand, the spectrum in V polarization, $S_V(\omega)$, plotted with a dashed blue line in Fig. 1(c), contains seven peaks corresponding to the nine possible transitions between dressed states, $|i\rangle \rightarrow |j\rangle$, with those three between the same dressed states, $|i\rangle \rightarrow |i\rangle$, degenerate in energy at ω_L .

TWO-PHOTON TRANSITIONS AND SPECTRUM

The next step in the characterization of the system is the calculation of the frequency-resolved second order correlation function or two-photon spectrum, $g_{\Gamma}^{(2)}(\omega_1, \omega_2)$ [50, 51], that conveys how likely is to detect two photons with frequencies ω_1, ω_1 simultaneously. For that purpose we use a recently developed technique [50] that makes the calculation of this quantity, previously very involved, computationally accessible, based on the

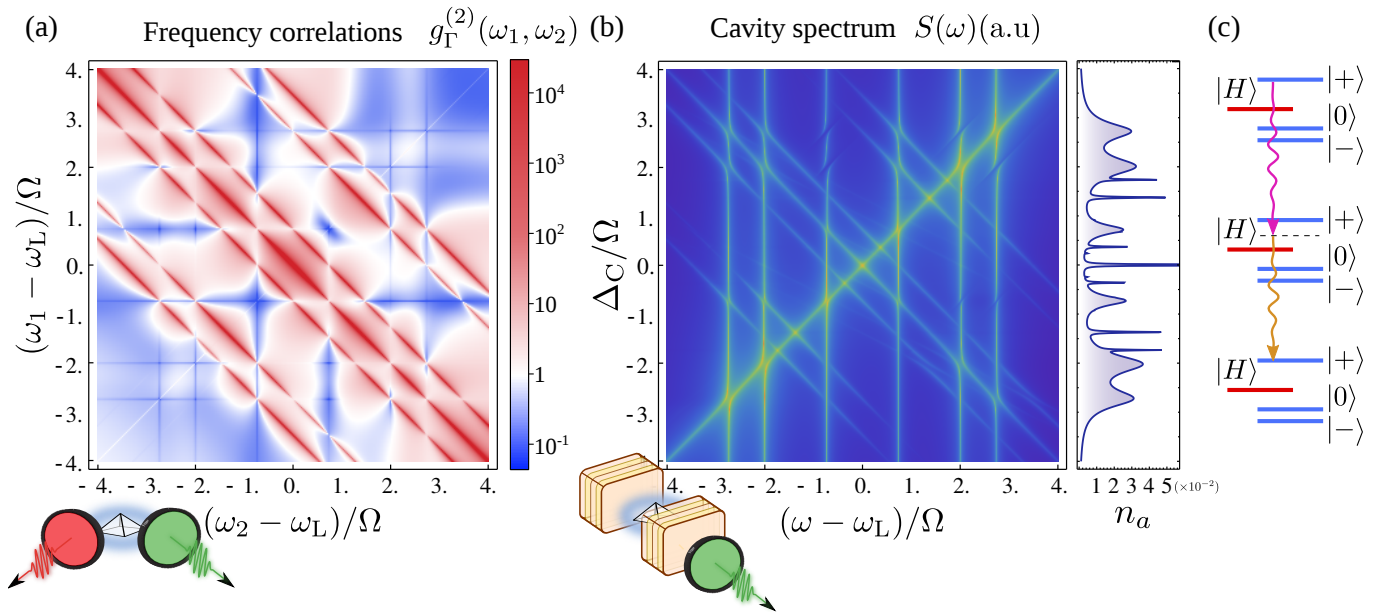


FIG. 2: (Color online) (a) Two-photon spectrum in H polarization for the TPE. In blue, sub-Poissonian statistics (antibunching), in red, super-Poissonian statistics (bunching) and in white, Poissonian statistics (uncorrelated). Parameters: $\chi = 4 \times 10^3 \gamma$, $\Omega = 10^3 \gamma$, $\Gamma = 10\gamma$ and $g = 0$. (b) Cavity spectrum of emission as a function of the cavity frequency ω_a in the strong coupling regime, $g = 10^2 \gamma$, $\kappa = 10\gamma$. The plot on the right hand side shows the integrated signal, i.e., the cavity population n_a . (c) Example of the two-photon transition $|+\rangle \rightarrow |+\rangle$ in the H polarization.

inclusion of the detectors in the system dynamics. The parameter Γ is the inverse response time of the detector. It provides the frequency window in which photons are detected around ω_1, ω_2 . We fix it to an intermediate value $\Gamma = 10\gamma$, so that the detectors can resolve full spectral peaks (with width of the order of γ) without resulting in superimposed signals, $\gamma < \Gamma \ll \Omega$.

Figure 2(a) shows the H-polarized two-photon spectrum from the light emitted by the dressed biexciton system. This map features seven antidiagonal red lines of super Poissonian correlations with $g_{\Gamma}^{(2)} \gg 1$ (hyperbunching) that correspond to a family of virtual two-photon processes that go from one state in a rung to another state two rungs below, jumping over any states from the rung in between (whence the denomination of *leapfrog* processes). It was recently demonstrated [42] that this virtual character provides such strong quantum correlations that photon pairs can violate classical inequalities such as the Cauchy-Schwarz inequality. Whenever any two of the frequencies involved correspond to transitions between real states, these correlations change character and the violation of Cauchy-Schwarz inequalities is spoiled. This can be seen in Fig. 2(a) as a piercing in the bunching lines whenever they intersect the vertical or horizontal ones, appearing at $\omega_{1,2} - \omega_L = \pm\Delta_I, \pm\Delta_{II}, \pm\Delta_{III}$.

Since the leapfrog lines originate from two-photon transitions, we can understand them in terms of the two-photon operator $\sigma_H \sigma_H$. Transitions starting or end-

ing at $|H\rangle$ are not allowed, since $|\langle H|\sigma_H \sigma_H|i\rangle| = 0$ and $|\langle i|\sigma_H \sigma_H|H\rangle| = 0$. All other nine two-photon transitions, $|i\rangle \rightarrow |j\rangle$, occur, since $|\langle j|\sigma_H \sigma_H|i\rangle| \neq 0$ for all $i, j = +, 0, -$, and give rise to seven lines which follow the general equation $\omega_1 + \omega_2 - 2\omega_L = \Delta^{2P}$ with:

$$|i\rangle \rightarrow |i\rangle \quad \text{with } i = +, 0, - : \quad \Delta_I^{2P} = 0, \quad (12a)$$

$$|+\rangle \rightarrow |0\rangle : \quad \Delta_{II}^{2P} = \frac{1}{8} \left(\sqrt{\chi^2 + 32\Omega^2} + \chi \right), \quad (12b)$$

$$|0\rangle \rightarrow |-\rangle : \quad \Delta_{III}^{2P} = \frac{1}{8} \left(\sqrt{\chi^2 + 32\Omega^2} - \chi \right), \quad (12c)$$

$$|+\rangle \rightarrow |-\rangle : \quad \Delta_{IV}^{2P} = \frac{1}{4} \sqrt{\chi^2 + 32\Omega^2}. \quad (12d)$$

The remaining three lines are described by inverting the order of the three last transitions and changing the sign of the corresponding Δ^{2P} . Figure 2(c) shows an example of a two-photon transition, $|+\rangle \rightarrow |+\rangle$.

In Fig. 3, we have another view of these leapfrog resonances, selecting the diagonal of the two-photon spectrum in Figure 2(a), that is, for $\omega = \omega_1 = \omega_2$. The leapfrog processes appear as seven lines around $\Omega/\chi \approx 10^{-1}$ and spread as Ω is increased. The blue lines correspond to the single-photon resonances that are also apparent in the spectrum of emission, c.f. Fig. 1(c). Reducing Ω below the dissipation levels (bottom part of the plot), the system experiences a transition into the spontaneous emission regime where there is no dressing of the levels and the spectral structures are much simpler: only two peaks for the spectrum of emission and a

single leapfrog peak at $\omega = \omega_L$ in the two-photon spectrum. This regime was extensively investigated by one of the authors under incoherent excitation [40]. In the present work, where it appears as the low pumping limit, it will be used only for comparison with the high pumping regime.

PURCELL ENHANCEMENT OF TWO-PHOTON TRANSITIONS BY A CAVITY MODE

These virtual leapfrog transitions can be made real by coupling the system to a cavity (we switch on $g \neq 0$) in resonance with at least one of the two frequencies involved. If the coupling is strong as compared to the cavity dissipation, κ , the two-photon emission can be Purcell-enhanced. We can observe this in the cavity spectrum of emission, given by $S_a(\omega) = \Re \int_0^\infty \langle a^\dagger(0)a(\tau) \rangle e^{i\omega\tau} d\tau$ and plotted in Fig. 2(b). Because of the strong correlations between the two frequencies, the cavity Purcell-enhancement of one of the two photons of a bunching line

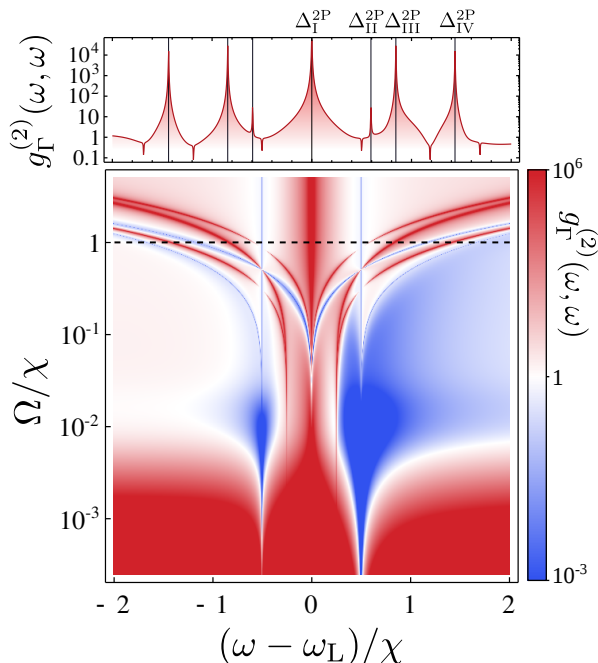


FIG. 3: (Color online) Two-photon spectrum with $\omega = \omega_1 = \omega_2$ (the diagonal) of the biexciton system as a function of the driving field intensity Ω . Top panel shows a cut along the dashed line in the bottom panel. Blue colors in the map represent sub-Poissonian statistics (antibunching), red, super-Poissonian statistics (bunching) and white, Poissonian statistics (uncorrelated). The physics changes from that of the biexciton spontaneous emission regime (bottom part), with a single leapfrog peak, to that of the dressed biexciton system (top part), with seven leapfrog peaks. Parameters: $\chi = 4 \times 10^3 \gamma$, $\Gamma = 10\gamma$ and $g = 0$.

triggers the emission of the second photon, even if this one is not in resonance with the cavity. This phenomenon leaves traces in the spectrum that help reconstruct the bunching lines when the spectrum is plotted as a function of the cavity frequency. In this sense, the cavity is acting as one of the filters necessary to perform frequency correlations.

As we have shown with coworkers in a recent work [39], one can obtain useful two-photon emission by using this approach to Purcell-enhance two photons of the same frequency. This is evidenced by sharp peaks in the cavity population whenever it crosses one of the two-photon resonances (Eqs. (12) with $\omega_a = \omega_1 = \omega_2$), as can be seen in the right panel of Fig. 2(b). The single photon resonances appear as broad peaks and are detrimental for the two-photon emission. Therefore, the best candidates for pure two-photon emission are those leapfrogs far in energy from other processes, that is, the sharp peaks with small overlap with the (one-photon) broad ones and that are further from other (two-photon) sharp ones. Logically, it is also desirable that they are intense. The central peak, labeled I, at $\omega_a = \omega_L$ is the best candidate since it is the most isolated one and is degenerate, with contributions from three different leapfrog processes. As we will discuss, this has consequences on the statistics of the emitted pairs.

An accurate quantity to determine the quality of a two-photon resonance for two-photon emission is the *purity*, π_2 [39], defined as the fraction of photons emitted in pairs from the total emission (including single photons). Note that the purity being a probability, it is, unlike $g^{(2)}$, bounded: $0 \leq \pi_2 \leq 1$. Its definition is based on the fact that the photon counting distribution of a perfect two-photon emitter shows a suppressed probability of counting an odd number of photons. The details of its definition and computation can be found in the Supplemental Material. In order to compute it, we simulate the actual emission of the system in the steady state via a quantum Monte-Carlo method [39]. The result is plotted in Fig. 4(d) for a cavity on resonance with each of the leapfrog peaks in the two-photon spectrum: I, II, III and IV, whose positions shift with Ω as plotted in panel (e). The corresponding cavity population $n_a = \langle a^\dagger a \rangle$, second order correlation function $g^{(2)}(0) = \langle a^{\dagger 2} a^2 \rangle / n_a^2$ and two-photon second order correlation function [39] $g_2^{(2)}(0) = \langle a^{\dagger 4} a^4 \rangle / \langle a^{\dagger 2} a^2 \rangle^2$ appear in (a), (b) and (c) respectively. The latter quantity takes the meaning of a standard *second order correlation function for photon pairs* when these pairs dominate the emission ($\pi_2 \approx 1$).

On the low driving regime, we can see that resonances I and II converge to the same point at $\omega = \omega_L$ and show very high purity: this is the usual regime of two-photon emission in the (undressed) biexciton, that has been studied extensively before [52, 53]. Note, however, that this

high purity comes at the expense of the amount of signal (low n_a). As Fig. 4 shows, this signal can be enhanced by orders of magnitude if we increase the pumping intensity Ω in order to bring the biexciton to the dressed regime. In this regime, all the resonances start being resolved and the four of them present a sizable purity. In the case of resonances II, III and IV, the purity goes down whenever they cross a single-photon resonance (dashed, vertical lines in Fig 4). At very high intensity, $\Omega > \chi$, all of them reach almost 100% of pair emission.

In this limit of high pumping, we observe a bunching behaviour $g^{(2)}(0) > 1$ for all the leapfrog resonances, which is an expected result for two-photon emission. The

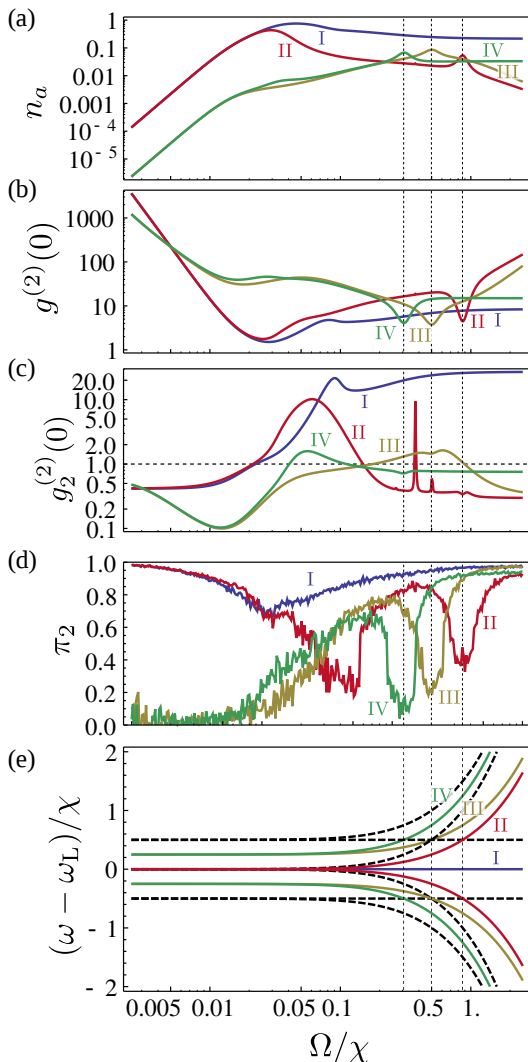


FIG. 4: (Color online) Steady state observables as a function of the pumping intensity Ω for the parameters: $\chi = 4 \times 10^3 \gamma$, $g = 10^2 \gamma$, $\kappa = 10 \gamma$, $\Delta_x = \chi/2$ and $\Delta_C = \Delta_I^{2P}$ (blue), Δ_{II}^{2P} (red), Δ_{III}^{2P} (yellow) and Δ_{IV}^{2P} (green). The gridlines mark the three points where leapfrog processes intersect with real transitions—dashed lines in (e)—, which spoils the purity.

statistics of the photons, however, hides a non-classical behaviour if one regards the pairs as the basic entity of emission and consider the pair-pair coincidences as described by the $g_2^{(2)}(0)$. In this case, we obtain *antibunched photon pairs* in resonances II, III and IV and *bunched photon pairs* in resonance I. This is not the only difference between resonance I (blue) and the others. The position of this resonance is independent of the pumping intensity, and the emission at this frequency is order of magnitudes more intense than at the other resonances. These differences are explained by the fact that three different transitions contribute to the photon pair emission at line I, and that the starting and ending state of the transition are always the same, as can be seen in Eq. (12a). Because of this, no reloading time to go back to the initial state is needed, which is the origin of the antibunching on all the other cases. All these features are a sample of the rich set of physical regimes that can be explored when the proposed method of multi-photon Purcell enhancement in dressed states systems is applied in non-trivial configurations.

EMISSION OF ENTANGLED PHOTONS

Many practical applications in quantum computing and quantum communication require emission of entangled photon pairs [3, 5–11]. So far, we have only considered the case in which the emission was filtered by a single cavity with a fixed polarization. Therefore, changing the frequency of the cavity corresponds to moving along the diagonal of Fig. 2(a), and all photons extracted by the cavity will tend to be indistinguishable. However, the results for the spectrum of the cavity emission depicted in Fig. 2(b) show that correlated photons of different frequencies can be Purcell enhanced with a single cavity: therefore, two cavities in resonance with two different, correlated frequencies—showing bunching in the map of Fig. (2)(a)—will be expected to show strongly correlated emission. In our case, another interesting possibility provided by the biexcitonic structure is to work with two degenerate polarizations of a single cavity, described by the bosonic annihilation operators a_H and a_V . Two-photon emission then takes place in a reduced Hilbert space of polarizations $\{|HH\rangle, |HV\rangle, |VH\rangle, |VV\rangle\}$ of photons with the same energy. We will now show how the mechanism of two-photon emission described so far can also yield emission of entangled photons of the kind $|\psi\rangle = (|HV\rangle + |VH\rangle)/\sqrt{2}$. The problem is theoretically described in the same way as before, but now with a different coupling Hamiltonian:

$$H_C = \omega_C(a_H^\dagger a_H + a_V^\dagger a_V) + g(a_H^\dagger \sigma_H + a_H \sigma_H^\dagger) + g(a_V^\dagger \sigma_V + a_V \sigma_V^\dagger) \quad (13)$$

The vertically polarized driving term (4) used above leads to different probability of emission in horizontal or vertical polarization. Since we now want equal probability, we use a circularly-polarized driving laser:

$$H_{\Omega} = \Omega (\sigma_{\circ}^{\dagger} e^{-i\omega_L t} + \sigma_{\circ} e^{i\omega_L t}) \quad (14)$$

with $\sigma_{\circ} = (\sigma_H + i\sigma_V)/\sqrt{2}$. We will not discuss in detail the possible single and two-photon transitions that arise in this model, since the physics and derivation are similar to the above material. However, it is now of interest to analyze the frequency-resolved, cross polarized second order correlation function $g_{\Gamma, \text{HV}}^{(2)}(\omega_1, \omega_2)$ of the dressed biexcitonic system alone ($g = 0$), which is a cross-correlation function between photons emitted at frequency ω_1 and polarization H and photons emitted at frequencies ω_2

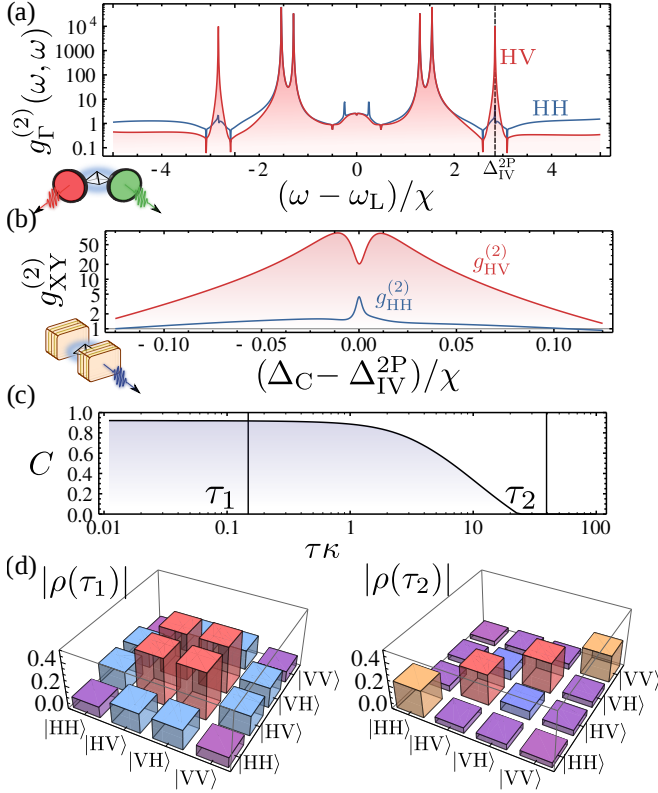


FIG. 5: (Color online) (a) Two photon spectrum for $\omega = \omega_1 = \omega_2$ (diagonal) of the dressed biexciton for photons with opposed polarization (red) and same polarization (blue). For photons emitted at frequency Δ_{IV}^{2P} , the cross correlation between polarizations is higher than the autocorrelations. (b) Autocorrelations and cross-correlations between two cavity modes with orthogonal polarizations coupled to the dressed biexciton as a function of their energy around Δ_{IV}^{2P} . (c) Concurrence of the emitted photon-pair state as a function of the total measurement time. (d) Density matrix of the emitted state for two different total measurement times denoted as τ_1 and τ_2 . Parameters: $\Omega = 8 \times 10^3 \gamma$, all the rest same as in Fig. 4.

and polarization V. This correlation function can be compared with the frequency-resolved correlation functions for a fixed polarization that we have been considering so far, that we now term $g_{\Gamma, \text{HH}}^{(2)}(\omega_1, \omega_2)$. Due to the circular polarized pumping, the system is symmetric under the exchange $H \leftrightarrow V$, so $g_{\Gamma, \text{HH}}^{(2)}(\omega_1, \omega_2) = g_{\Gamma, \text{VV}}^{(2)}(\omega_1, \omega_2)$ and $g_{\Gamma, \text{HV}}^{(2)}(\omega_1, \omega_2) = g_{\Gamma, \text{VH}}^{(2)}(\omega_1, \omega_2)$.

Figure 5(a) shows the comparison between these two quantities, with both photons having the same frequency ($\omega_1 = \omega_2 = \omega$), equivalent to Fig. 3, which was for the case of linearly polarized pumping. We observe that photons emitted at a frequency $\omega = \omega_L + \Delta_{IV}^{2P}$ present strong cross-polarized correlations, clearly higher than the autocorrelation for each polarization. This is a non-classical result that violates the Cauchy-Schwarz inequality [42, 54]. When the two degenerate modes described by a_H and a_V are tuned to $\omega_L + \Delta_{IV}^{2P}$ and coupled to the system as described in Eq. (13), their cross correlation $g_{\text{HV}}^{(2)} = \langle a_H^{\dagger} a_V^{\dagger} a_H a_V \rangle / (\langle a_H^{\dagger} a_H \rangle \langle a_V^{\dagger} a_V \rangle)$ and autocorrelation $g_{\text{HH}}^{(2)} = \langle a_H^{\dagger} a_H^{\dagger} a_H a_H \rangle / \langle a_H^{\dagger} a_H \rangle^2$ replicate the trend just described for the frequency-resolved second order correlations of the dressed biexciton alone. This can be seen in Figure 5(b), where the auto and cross-correlations of the two cavity modes are shown for a range of cavity frequencies around $\omega_L + \Delta_{IV}^{2P}$.

Quantum tomography [27, 40, 55, 56] allows us to reconstruct the density matrix of the emitted photon pairs in the basis $\{|HH\rangle, |HV\rangle, |VH\rangle, |VV\rangle\}$ from second order correlation functions corresponding to photon coincidence measurements. We define the (unnormalized) density matrix:

$$\theta_{\text{AB,CD}}(\tau) = \int_0^{\tau} \langle a_A^{\dagger}(0) a_B^{\dagger}(\tau') a_D(\tau') a_C(0) \rangle d\tau' \quad (15)$$

with $A, B, C, D \in \{H, V\}$, where two-time correlation functions are calculated from the steady state of the system using the quantum regression theorem [57]. Therefore, τ corresponds to the time of measurement that begins with the emission of the first photon, and for each τ we define the normalized density matrix $\tilde{\theta}(\tau) = \theta(\tau) / \text{Tr}[\theta(\tau)]$. This analysis reveals, for short measurement times, a highly pure density matrix, $\text{Tr}[\tilde{\theta}^2] \approx 0.92$ consisting of the entangled Bell state $|\psi\rangle = (|HV\rangle + |VH\rangle)/\sqrt{2}$ with fidelity $F \approx 0.9$, shown in Fig. 5(d). Beyond a certain time of measurement $1/\kappa$, the density matrix loses purity due to the contributions from subsequent emissions. The degree of entanglement of this emitted bipartite state can be quantified by the concurrence C [60], that in the case of pure states ranges from 0 (separable states) to 1 (maximally entangled states) [58]. In our case, the concurrence takes a value $C \approx 0.92$ for short measurement times. However, one must bear in mind that the maximum concurrence for a mixed state is lower than one [59] and $\tilde{\theta}$ is a mixed state with linear entropy $S_L(\tilde{\theta}) = 4/3[1 - \text{Tr}(\tilde{\theta}^2)] \approx 0.11$, which brings

this value of C closer to that of a maximally entangled mixed state. Not only is this result interesting by itself, but, being just a particular example, it also suggests that photons entangled not only in the polarization, but also in the energy degree of freedom—which in this case has been chosen equal for both photons for simplicity—could be obtained.

CONCLUSIONS

We have shown how Purcell enhancement of multiphoton resonances in the dressed ladder of a strongly driven biexciton can yield regimes of bright continuous two-photon emission. Thanks to the strong driving, the emission of photon pairs occurs at a much higher rate than it would in the approach that combines standard TPE (without dressing the system) and two-photon Purcell enhancement. The richness of the dressed biexcitonic structure allows to reach different two photon regimes like antibunched two-photon emission or entangled photon pairs. These results suggest that the fundamental ideas behind this particular proposal are susceptible to be applied in a variety of platforms.

ACKNOWLEDGMENTS

We acknowledge the IEF project SQUIRREL (623708), the Spanish MINECO (MAT2011-22997, MAT2014-53119-C2-1-R, FPI & RyC programs) and the ERC PO-LAFLOW.

-
- [1] O'Brien, J. L., Furusawa, A. & Vuckovic, J. Photonic quantum technologies. *Nat. Phys.* **3**, 687 (2009).
- [2] Knill, E., Laflamme, R. & Milburn, G. J. A scheme for efficient quantum computation with linear optics. *Nature* **409**, 46–52 (2001).
- [3] Pan, J.-W. *et al.* Multiphoton entanglement and interferometry. *Rev. Mod. Phys.* **84**, 777 (2012).
- [4] Hong, C. K. & Mandel, L. Experimental realization of a localized one-photon state. *Phys. Rev. Lett.* **56**, 58 (1986).
- [5] Jennewein, T., Simon, C., Weihs, G., Weinfurter, H. & Zeilinger, A. Quantum cryptography with entangled photons. *Phys. Rev. Lett.* **84**, 4729 (2000).
- [6] Naik, D. S., Peterson, C. G., White, A. G., Berglund, A. J. & Kwiat, P. G. Entangled state quantum cryptography: Eavesdropping on the ekert protocol. *Phys. Rev. Lett.* **84**, 4733 (2000).
- [7] Bouwmeester, D. *et al.* Experimental quantum teleportation. *Nature* **390**, 575 (1997).
- [8] Marcikic, I., Riedmatten, H. D., Tittel, W., Zbinden, H. & Gisin, N. Long-distance teleportation of qubits at telecommunication wavelengths. *Nature* **421**, 509 (2003).
- [9] Pan, J.-W., Bouwmeester, D., Weinfurter, H. & Zeilinger, A. Experimental entanglement swapping: Entangling photons that never interacted. *Phys. Rev. Lett.* **80**, 3891 (1998).
- [10] Simon, C. *et al.* Quantum repeaters with photon pair sources and multimode memories. *Phys. Rev. Lett.* **98**, 190503 (2007).
- [11] Troiani, F. Entanglement swapping with energy-polarization-entangled photons from quantum dot cascade decay. *Phys. Rev. B* **90**, 245419 (2014).
- [12] Giovannetti, V., Lloyd, S. & Maccone, L. Quantum-enhanced measurements: Beating the standard quantum limit. *Science* **306**, 1330 (2004).
- [13] Gea-Banacloche, J. Two-photon absorption of nonclassical light. *Phys. Rev. Lett.* **62**, 1603 (1989).
- [14] Upton, L. *et al.* Optically excited entangled states in organic molecules illuminate the dark. *The Journal of Physical Chemistry Letters* **4**, 2046–2052 (2013).
- [15] Peruzzo, A. *et al.* Quantum walks of correlated photons. *Science* **329**, 1500 (2010).
- [16] Lanyon, B. P. *et al.* Towards quantum chemistry on a quantum computer. *Nat. Chem.* **2**, 106 (2010).
- [17] Burnham, D. C. & Weinberg, D. L. Observation of simultaneity in parametric production of optical photon pairs. *Phys. Rev. Lett.* **25**, 84 (1970).
- [18] Kwiat, P. G. *et al.* New high-intensity source of polarization-entangled photon pairs. *Phys. Rev. Lett.* **75**, 4337 (1995).
- [19] Lanco, L. *et al.* Semiconductor waveguide source of counterpropagating twin photons. *Phys. Rev. Lett.* **97**, 173901 (2006).
- [20] Horn, R. *et al.* Monolithic source of photon pairs. *Phys. Rev. Lett.* **108**, 153605 (2012).
- [21] Boitier, F. *et al.* Electrically injected photon-pair source at room temperature. *Phys. Rev. Lett.* **112**, 183901 (2014).
- [22] Scarani, V., Riedmatten, H. D., Marcikic, I., Zbinden, H. & Gisin, N. Four-photon correction in two-photon bell experiments. *The European Physical Journal D-Atomic, Molecular, Optical and Plasma Physics* **32**, 129 (2005).
- [23] Aspect, A., Grangier, P. & Roger, G. Experimental tests of realistic local theories via bell's theorem. *Phys. Rev. Lett.* **47**, 460 (1981).
- [24] Stevenson, R. M. *et al.* A semiconductor source of triggered entangled photon pairs. *Nature* **439**, 179 (2006).
- [25] Akopian, N. *et al.* Entangled photon pairs from semiconductor quantum dots. *Phys. Rev. Lett.* **96**, 130501 (2006).
- [26] Hafenbrak, R. *et al.* Triggered polarization-entangled photon pairs from a single quantum dot up to 30K. *New J. Phys.* **9**, 315 (2007).
- [27] Dousse, A. *et al.* Ultrabright source of entangled photon pairs. *Nature* **466**, 217 (2010).
- [28] Müller, M., Bounouar, S., Jöns, K. D., Glässl, M. & Michler, P. On-demand generation of indistinguishable polarization-entangled photon pairs. *Nat. Photon.* **8**, 224–228 (2014).
- [29] Flissikowski, T., Betke, A., Akimov, I. A. & Henneberger, F. Two-photon coherent control of a single quantum dot. *Phys. Rev. Lett.* **92**, 227401 (2004).
- [30] Stuffer, S. *et al.* Two-photon Rabi oscillations in a single $\text{In}_x\text{Ga}_{1-x}\text{As}/\text{GaAs}$ quantum dot. *Phys. Rev. B* **73**, 125304 (2006).
- [31] Jayakumar, H. *et al.* Deterministic photon pairs and

- coherent optical control of a single quantum dot. *Phys. Rev. Lett.* **110**, 135505 (2013).
- [32] Huber, T. *et al.* Coherence and degree of time-bin entanglement from quantum dots. *arXiv:1506.02429* (2015).
- [33] Birowosuto, M. D. *et al.* Fast purcell-enhanced single photon source in 1,550-nm telecom band from a resonant quantum dot-cavity coupling. *Scientific Report* **2** (2012).
- [34] del Valle, E. *et al.* Two-photon lasing by a single quantum dot in a high- Q microcavity. *Phys. Rev. B* **81**, 035302 (2010).
- [35] Ota, Y., Iwamoto, S., Kumagai, N. & Arakawa, Y. Spontaneous two-photon emission from a single quantum dot. *Phys. Rev. Lett.* **107**, 233602 (2011).
- [36] Schumacher, S. *et al.* Cavity-assisted emission of polarization-entangled photons from biexcitons in quantum dots with fine-structure splitting. *Opt. Express* **20**, 5335 (2012).
- [37] Cohen-Tannoudji, C. N. & Reynaud, S. Dressed-atom description of resonance fluorescence and absorption spectra of a multi-level atom in an intense laser beam. *J. Phys. B.: At. Mol. Phys.* **10**, 345 (1977).
- [38] Muller, A., Fang, W., Lawall, J. & Solomon, G. S. Emission spectrum of a dressed exciton-biexciton complex in a semiconductor quantum dot. *Phys. Rev. Lett.* **101**, 027401 (2008).
- [39] Sánchez Muñoz, C. *et al.* Emitters of N -photon bundles. *Nat. Photon.* **8**, 550 (2014).
- [40] del Valle, E. Distilling one, two and entangled pairs of photons from a quantum dot with cavity QED effects and spectral filtering. *New J. Phys.* **15**, 025019 (2013).
- [41] Gonzalez-Tudela, A., del Valle, E. & Laussy, F. P. Optimization of photon correlations by frequency filtering. *Phys. Rev. A* **91**, 043807 (2015).
- [42] Sánchez Muñoz, C., del Valle, E., Tejedor, C. & Laussy, F. P. Violation of classical inequalities by photon frequency filtering. *Phys. Rev. A* **90**, 052111 (2014).
- [43] Peiris, M. *et al.* Two-color photon correlations of the light scattered by a quantum dot. *Phys. Rev. B* **91**, 195125 (2015).
- [44] Quang, T. & Freedhoff, H. Atomic population inversion and enhancement of resonance fluorescence in a cavity. *Phys. Rev. A* **47**, 2285 (1993).
- [45] Kim, H., Shen, T. C., Roy-Choudhury, K., Solomon, G. S. & Waks, E. Resonant interactions between a mollow triplet sideband and a strongly coupled cavity. *Phys. Rev. Lett.* **113**, 027403 (2014).
- [46] Aspect, A., Roger, G., Reynaud, S., Dalibard, J. & Cohen-Tannoudji, C. Time correlations between the two sidebands of the resonance fluorescence triplet. *Phys. Rev. Lett.* **45**, 617 (1980).
- [47] Schrama, C. A., Nienhuis, G., Dijkerman, H. A., Stejsiger, C. & Heideman, H. G. M. Intensity correlations between the components of the resonance fluorescence triplet. *Phys. Rev. A* **45**, 8045 (1992).
- [48] Ulhaq, A. *et al.* Cascaded single-photon emission from the Mollow triplet sidebands of a quantum dot. *Nat. Photon.* **6**, 238 (2012).
- [49] Baur, M. *et al.* Measurement of autler-townes and mollow transitions in a strongly driven superconducting qubit. *Phys. Rev. Lett.* **102**, 243602 (2009).
- [50] del Valle, E., Gonzalez-Tudela, A., Laussy, F. P., Tejedor, C. & Hartmann, M. J. Theory of frequency-filtered and time-resolved n -photon correlations. *Phys. Rev. Lett.* **109**, 183601 (2012).
- [51] Gonzalez-Tudela, A., Laussy, F. P., Tejedor, C., Hartmann, M. J. & del Valle, E. Two-photon spectra of quantum emitters. *New J. Phys.* **15**, 033036 (2013).
- [52] del Valle, E., Gonzalez-Tudela, A., Cancellieri, E., Laussy, F. P. & Tejedor, C. Generation of a two-photon state from a quantum dot in a microcavity. *New J. Phys.* **13**, 113014 (2011).
- [53] del Valle, E., Gonzalez-Tudela, A. & Laussy, F. P. Generation of a two-photon state from a quantum dot in a microcavity under incoherent and coherent continuous excitation. *Proc. SPIE* **8255**, 825505 (2012).
- [54] Reid, M. D. & Walls, D. F. Violations of classical inequalities in quantum optics. *Phys. Rev. A* **34**, 1260 (1986).
- [55] James, D. F. V., Kwiat, P. G., Munro, W. J. & White, A. G. Measurement of qubits. *Phys. Rev. A* **64**, 52312 (2001).
- [56] Troiani, F., Perea, J. I. & Tejedor, C. Cavity-assisted generation of entangled photon pairs by quantum dot cascade decay. *Phys. Rev. B* **74**, 235310 (2006).
- [57] Scully, M. O. & Zubairy, M. S. *Quantum optics* (Cambridge University Press, 2002).
- [58] Wootters, W. K. Entanglement of formation of an arbitrary state of two qubits. *Phys. Rev. Lett.* **80**, 2245 (1998).
- [59] Wei, T. C. *et al.* Maximal entanglement versus entropy for mixed quantum states. *Phys. Rev. A* **67**, 022110 (2003).
- [60] This quantity is defined as $C = \max\{0, \sqrt{\lambda_1} - \sqrt{\lambda_2} - \sqrt{\lambda_3} - \sqrt{\lambda_4}\}$, where $\{\lambda_1, \lambda_2, \lambda_3, \lambda_4\}$ are the eigenvalues in decreasing order of the matrix $\rho T \rho^* T$, with T a diagonal matrix with diagonal $\{-1, 1, 1, -1\}$.

Enhanced two-photon emission from a dressed biexciton. Supplemental Material

In this Supplemental Material we define the *purity* π , a magnitude that quantifies the percentage of photons emitted in pairs from the total emission. This is therefore a bounded quantity $\pi \in [0, 1]$, and its definition is based on the observation that a perfect two-photon emitter will never emit an odd number of photons. We start the discussion by describing the probability distribution of the sum of two random variables in terms of generating functions. In our case, these two random variables correspond to the number of photons emitted by two different processes: one emits photons one by one, and the other, in pairs. The entirety of the light emitted is assumed to be the sum of these two processes, and we will show how this assumption does describes very accurately the photon counting distributions of the light emitted by the system.

SUM OF TWO RANDOM PROCESSES

For a given discrete random process X , we can define the generating function $\Pi_X = \langle s^X \rangle$, in such a way that the probability of obtaining X is given by $P(X) = \frac{1}{n!} \partial^{(x)} / \partial s^x \Pi_X |_{s=0}$. When we combine different random processes, the generating function is given by the product of the two original ones: $\Pi_{X_1+X_2} = \Pi_{X_1} \Pi_{X_2}$. In the case of a coherent random process, the generating function is given by $\Pi_\lambda = e^{-\lambda(1-s)}$. As we will see, this exponential form will be convenient. For the purpose of obtaining a general expression for the n -th derivative needed to compute $P(X)$ from the generating function, we will use Faà di Bruno's formula for the generalized chain rule expressed in term of Bell polynomials $B_{n,k}(x_1, \dots, x_{n-k+1})$:

$$\frac{d^n}{dx^n} f(g(x)) = \sum_{k=1}^n f^{(k)}(g(x)) B_{n,k} \left(g'(x), g''(x), \dots, g^{(n-k+1)}(x) \right). \quad (S1)$$

If f , as is the case for the coherent process, is just the exponential function, the n -th derivative of f appearing in (S1) can be taken out of the sum, which becomes just the sum of Bell polynomials known as the complete Bell polynomial $B_n(a_1, \dots, a_n) = \sum_{k=1}^n B_{n,k}(a_1, \dots, a_{n-k+1})$. Therefore, for a generating function of the form $\Pi_n = e^{g(s)}$, the corresponding probability for the random process is:

$$P(n) = \frac{1}{n!} \frac{d^n}{ds^n} \Pi_n |_{s=0} = \frac{e^{g(0)}}{n!} B_n(a_1, \dots, a_n) \quad (S2)$$

with $a_n = g^{(n)}(0)$, and $B_0(\{\}) = 1$. This reduces the problem of obtaining the photon counting distribution for a combination of random processes to express the generating function as a single exponential $e^{g(s)}$ and computing the n -th derivative of the exponent $g^{(n)}(0)$.

THERMAL AND COHERENT DISTRIBUTIONS

The approach to quantify the fraction of two-photon emission requires the selection of a proper ansatz for the photon counting distributions of single and two-photon processes, see Fig. S1. For the case under discussion, we have obtained good results by considering a coherent one-photon distribution, a coherent two-photon distribution and a thermal two-photon distribution. The thermal component is essential to describe the photon counting distributions along the leapfrog line Δ_I^{2P} , giving incorrect results otherwise (see Fig. S1). The generating functions for a coherent one-photon process (λ_1), a coherent two-photon process (λ_2) and a thermal two-photon process (θ_2) are given by:

$$\Pi_{\lambda_1} = e^{-\lambda_1(1-s)} \quad (S3)$$

$$\Pi_{\lambda_2} = e^{-\lambda_2(1-s^2)} \quad (S4)$$

$$\Pi_{\theta_2} = \frac{1 - \theta_2}{1 - s^2 \theta_2} = e^{\log \left(\frac{1 - \theta_2}{1 - s^2 \theta_2} \right)} \quad (S5)$$

This give the total generating function $\Pi_{\lambda_1, \lambda_2, \theta_2} = \Pi_{\lambda_1} \Pi_{\lambda_2} \Pi_{\theta_2} = e^{g(s)}$, with

$$g(s) = -\lambda_1(1-s) - \lambda_2(1-s^2) + \log \left(\frac{1 - \theta_2}{1 - s^2 \theta_2} \right) \quad (S6)$$

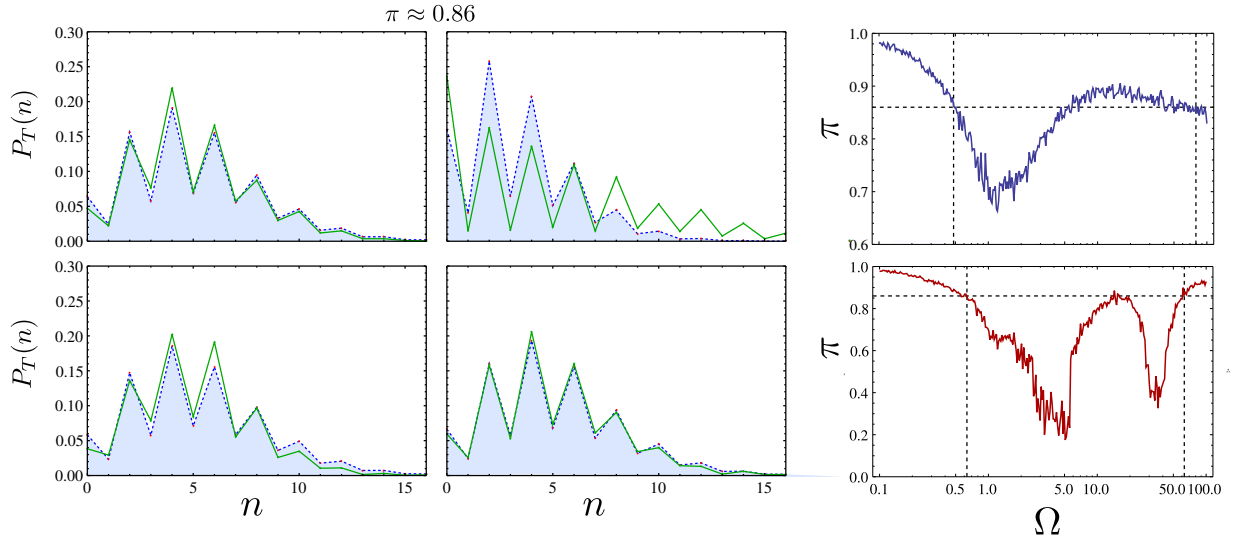


FIG. S1: Photon counting distributions with the same purity according to some ansatz (in this case, coherent single and two photon processes) are sometimes badly fit. Upper row: Δ_I^{2P} . Lower row: Δ_{II}^{2P} . The case of higher Ω for Δ_I^{2P} shows the ansatz is not correct in this case.

whose n -th derivatives are:

$$g^{(n)}(0) = \delta_{n,1} \lambda_1 + \delta_{n,2} 2\lambda_2 + \begin{cases} \theta_2^{n/2} 2[(n-1)!] & n \text{ even} \\ 0 & n \text{ odd} \end{cases} \quad (\text{S7})$$

This is all the information one needs to construct the photon counting probability given by Eq. (S2).

THERMAL AND COHERENT COMPONENTS OF THE PURITY

By fitting Monte Carlo photon counting curves such as the ones shown in Fig. S1 one can obtain values for the parameters λ_1 , λ_2 and θ_2 for a given time window T . The mean values associated with each of the three processes are $\bar{n}_{\lambda_1} = \lambda_1$, $\bar{n}_{\lambda_2} = \lambda_2$ and $\bar{n}_{\theta_2} = \theta_2/(1-\theta_2)$. The purity can then be defined as the fraction of the total mean value which is given by two-photon processes, that is:

$$\pi = \frac{\bar{n}_{\lambda_2} + \bar{n}_{\theta_2}}{\bar{n}_{\lambda_1} + \bar{n}_{\lambda_2} + \bar{n}_{\theta_2}} = \frac{\theta_2/(1-\theta_2) + \lambda_2}{\lambda_1 + \lambda_2 + \theta_2/(1-\theta_2)}. \quad (\text{S8})$$

This purity can be divided in a thermal plus a coherent part, $\pi = \pi_\theta + \pi_\lambda$, given by:

$$\pi_\theta = \frac{\theta_2/(1-\theta_2)}{\lambda_1 + \lambda_2 + \theta_2/(1-\theta_2)} \quad (\text{S9})$$

$$\pi_\lambda = \frac{\lambda_2}{\lambda_1 + \lambda_2 + \theta_2/(1-\theta_2)} \quad (\text{S10})$$

The result of using the cothermal ansatz (S7) for the photon counting distribution and computing the purity as given by (S8) for the central leapfrog Δ_I^{2P} in the biexciton configuration is summarized in Fig. S2. This provides the expected result of the purity being corresponding to that of a thermal process of bundle emission, which matches the bunched values of $g_2^{(2)}(0)$ in this line. Figure S3 shows the associated errors in the fittings, demonstrating that the cothermal fit provides much better results.

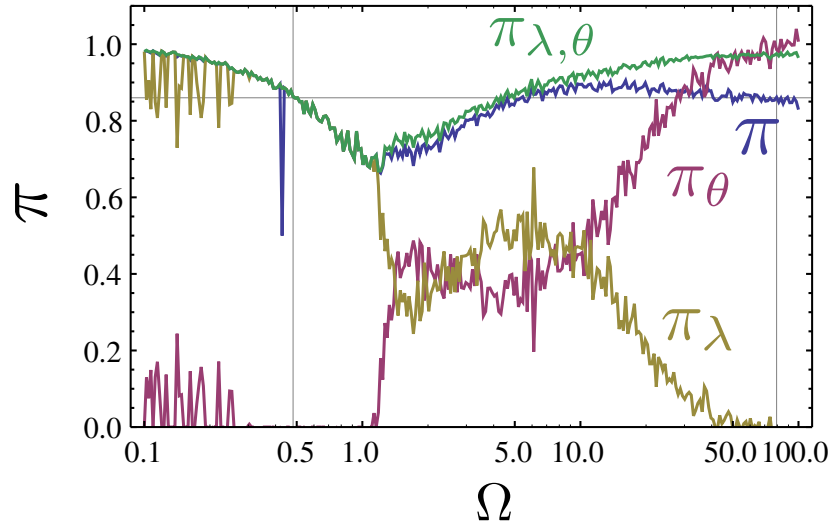


FIG. S2: Purity for the central leapfrog as calculated by the standard method (π) and by the cothermal ansatz ($\pi_{\lambda,\theta}$), also with the separated thermal and coherent contributions. We see how the thermal contribution becomes important in this case and gives a higher purity than the one obtained with the standard, coherent ansatz.

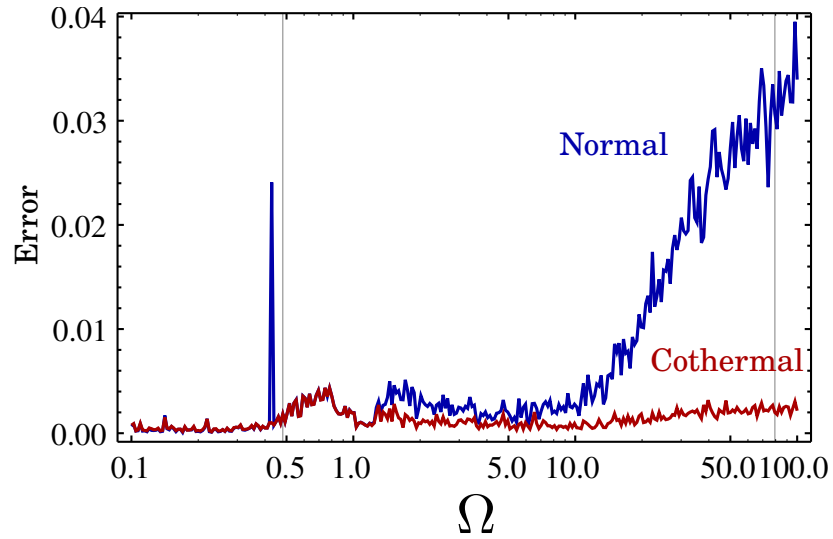


FIG. S3: Error of the fitting procedure for the central leapfrog when using the standard coherent ansatz (blue) and the cothermal ansatz (red). This shows that the second method gives a much better fitting.